Hydrogen Dynamics in Na_3AlH_6: A Combined Density Functional Theory and Quasielastic Neutron Scattering Study

J. Voss,[†,‡] Q. Shi,[†,§] H. S. Jacobsen,[†,§] M. Zamponi,[||] K. Lefmann,[†] and T. Vegge*[,†]

Materials Research Department, Risø National Laboratory, Technical University of Denmark, DK-4000 Roskilde, Denmark, Center for Atomic-Scale Materials Design, Technical University of Denmark, DK-2800 Kongens Lyngby, Denmark, Niels Bohr Institute, University of Copenhagen, DK-1017 Copenhagen, Denmark, Institut für Festkörperforschung, Forschungszentrum Jülich, D-52425 Jülich, Germany

Received: October 12, 2006; In Final Form: January 29, 2007

Understanding the elusive catalytic role of titanium-based additives on the reversible hydrogenation of complex hydrides is an essential step toward developing hydrogen storage materials for the transport sector. Improved bulk diffusion of hydrogen is one of the proposed effects of doping sodium alanate with $TiCl_3$, and here we study hydrogen dynamics in doped and undoped Na_3AlH_6 using a combination of density functional theory calculations and quasielastic neutron scattering. The hydrogen dynamics is found to be vacancy mediated and dominated by localized jump events, whereas long-range bulk diffusion requires significant activation. The fraction of mobile hydrogen is found to be small for both undoped and doped Na_3AlH_6, even at 350 K, and improved hydrogen diffusion as a result of bulk-substituted titanium is found to be unlikely. We also propose that previously detected low-temperature point defect motion in sodium alanate could result from vacancy-mediated sodium diffusion.

1. Introduction

In 1997, Bogdanović and Schwickardi[1] showed that sodium alanate doped with titanium is cyclically dis- and rechargeable with hydrogen under near-ambient conditions. $NaAlH_4$ decomposes in two steps:

$$NaAlH_4 \leftrightarrow \frac{1}{3}Na_3AlH_6 + \frac{2}{3}Al + H_2$$
$$\leftrightarrow NaH + Al + \frac{3}{2}H_2 \quad (1)$$

where the two steps release 3.7 and 1.9 wt % of hydrogen, respectively. The decomposition temperature of NaH is generally too high for hydrogen storage applications.[2]

Despite intense research efforts, the physical understanding of the catalytic role of titanium on the improved hydrogen ab- and desorption kinetics has remained elusive, possibly due to a multiplicity in effects.[3−6]

A number of different models have been proposed to describe the catalytic effect of titanium, one of which is the formation of catalytic Al_xTi_y complexes at the surface,[7] improving either dissociation and recombination of molecular hydrogen or mass transport; a second model suggests bulk substitution of titanium for aluminum or sodium atoms, whereby hydrogen diffusion can be improved.[8]

Recent anelastic spectroscopy experiments on thermally treated sodium alanate samples reveal fast point defect dynamics at $T = 70$ K with a much larger fraction of mobile species for titanium-doped samples, therefore appearing to support the model of improved hydrogen diffusion due to bulk-substituted titanium.[9] This anelastic feature is expected to occur in the Na_3AlH_6 phase.[10]

In this paper, we focus on bulk hydrogen dynamics in the intermediate product Na_3AlH_6. By combining density functional theory (DFT) calculations and quasielastic neutron scattering (QENS), we find the hydrogen dynamics to be vacancy mediated and dominated by localized events. The mobile hydrogen fraction is found to be low for both undoped and Ti-doped Na_3AlH_6, and long-range bulk diffusion requires significant activation. Improved hydrogen diffusion due to bulk-substituted titanium[8] is found to be unlikely.

2. Theoretical Method

The electronic structure is calculated using density functional theory[12] in the DACAPO plane wave basis set implementation.[13] The ion cores are described by ultrasoft pseudopotentials.[14] The exchange and correlation effects are described by the PW91 functional.[15] The Kohn−Sham wavefunctions[12] are expanded in a plane wave basis set with a cutoff energy of 340 eV (for the density grid, a cutoff of 600 eV is used). The wave functions are sampled on a *k*-point mesh of spacing ~ 0.3 Å^{-1} in all three directions.

The total energy of the system and the Hellmann−Feynman forces on the ion cores are minimized using a quasi-Newton method.[16] To calculate the optimum crystal structure for $T = 0$ K, both atomic coordinates and unit cell parameters are relaxed iteratively. The resulting structural parameters for $P2_1/n$ -Na_3AlH_6 (space group no. 14) are presented in Table 1 (the values for β tend to vary insignificantly between different calculations[2,17−19] and experiment[20]).

For the calculation of formation and activation energies, we use computational ($2 \times 2 \times 1$) supercells with volume $2 \cdot 5.27 \times 2 \cdot 5.46 \times 7.60$ Å^3, containing 80 atoms.

* Corresponding author. E-mail: tejs.vegge@risoe.dk.
[†] Materials Research Department, Risø National Laboratory, Technical University of Denmark.
[‡] Center for Atomic-scale Materials Design, Technical University of Denmark.
[§] Niels Bohr Institute, University of Copenhagen.
[||] Institut für Festkörperforschung, Forschungszentrum Jülich.

10.1021/jp0667036 CCC: $37.00
Published on Web 03/24/2007

TABLE 1: Calculated Structural Parameters for $P2_1/n$-Na_3AlH_6 (Experimental Values from ref 20 in Parentheses)

unit cell parameters [Å]	
$a = 5.27$	(5.39)
$b = 5.46$	(5.514)
$c = 7.60$	(7.725)
$\beta = 89.99°$	(89.86°)
Wyckoff positions	
Al(2*a*)	0, 0, 0
Na(2*b*)	0, 0, 0.5
Na(4*e*)	−0.010, 0.454, 0.255 (−0.006, 0.461, 0.252)
H(4*e*)	0.102, 0.051, 0.218 (0.091, 0.041, 0.215)
H(4*e*)	0.226, 0.329, 0.544 (0.234, 0.328, 0.544)
H(4*e*)	0.162, 0.269, 0.934 (0.165, 0.266, 0.944)

In the calculational setup, vacancies are created by removing an atom from the supercell and re-relaxing the atomic coordinates. Two such vacancy configurations are then considered as initial and final state of a vacancy-mediated diffusion process, respectively.

A path technique known as the nudged elastic band (NEB) method[21] is used to accurately determine activation energies for the hydrogen dynamics. Here, the reaction path is represented by a finite number of configurations. An initial guess for the coordinates of the intermediate images of the system is a linear interpolation between the initial and final states. This path is then relaxed to the minimum energy path on the potential energy surface. The NEB consists of the configurations connected by springs, which stabilize the distances between the images. Only spring forces parallel to the path are considered in order to avoid perturbation of the curved path. Atomic forces are considered only perpendicular to the path, such that the energy gradients dragging the intermediate images to the initial and final states are mapped out, respectively.

For the accurate localization of transition states, i.e., local maxima of the minimum energy path, a modification of the NEB approach is used: the adaptive nudged elastic band (ANEB) method.[22] In this approach, subpaths consisting of only five configurations are relaxed iteratively, where the internal subpath containing the current configuration with highest energy is replaced by a refined subpath. Therefore, this method will generally find the transition state of a simple path with only one maximum.

For thermally activated processes like those investigated here, the activation energy E_a, i.e., the difference between the ground-state energy of initial and transition state, enters the reaction rate in a Boltzmann factor. The corresponding relation is known as the Arrhenius equation:

$$\tau^{-1} = \tau_0^{-1} \exp\left(-\frac{E_a}{k_B T}\right) \tag{2}$$

The prefactor τ_0^{-1} is determined by the ratio of the partition functions of the transition and initial state, respectively.[23] In harmonic transition state theory (hTST),[23] the prefactor only depends on the eigenfrequencies of the initial and transition state:

$$\tau_{0,\mathrm{TST}}^{-1} = \frac{1}{2\pi} \frac{\prod_i \omega_i^{\mathrm{I}}}{\prod_j{}' \omega_j^{\mathrm{T}}} \tag{3}$$

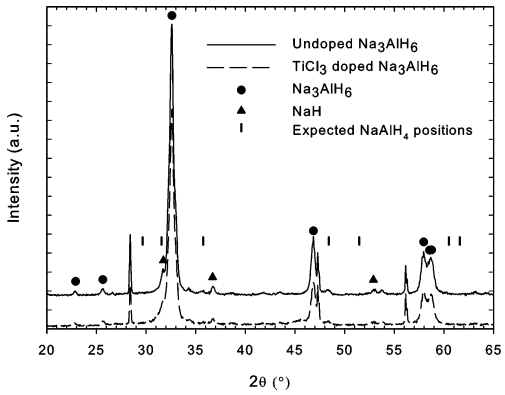

Figure 1. X-ray powder diffraction spectra of $NaAlH_4 + 2NaH$ mixture ball-milled 5 h (upper) and 4.5 h continued another half hour with addition of $TiCl_3$ (lower). The sharp peaks at 28.44°, 47.30°, and 56.12° stem from the Si reference sample.

where the prime denotes that the imaginary frequency at the transition state corresponding to the unstable eigenmode in the direction of the reaction coordinate is left out. The harmonic approximation has previously been shown even to be able to treat complex systems and elevated temperatures.[24,25]

The eigenfrequencies are calculated by mass-weighting the diagonalized Hessian of the total energy. The Hessian is determined by calculating the Hellmann−Feynman forces for configurations, with each atom displaced in one direction.

3. Experimental Methods

The Na_3AlH_6 samples were synthesized by energetic ball-milling of stoichiometric mixtures of NaH and $NaAlH_4$ as proposed by Hout et al.[26] $NaAlH_4$ (Sigma-Aldrich, 90%), NaH (Sigma-Aldrich, 95%), and the catalyst precursor, $TiCl_3$ (Alfa Aesar, $TiCl_3 \cdot {}^1/_3AlCl_3$, purity 76−78% $TiCl_3$) were used as received in powder form. The pure Na_3AlH_6 sample (sample I) was prepared by ball-milling of stoichiometric mixtures of NaH and $NaAlH_4$ for 5 h. In sample II, 4 mol % $TiCl_3$ was added to a mixture of $NaAlH_4$ and NaH, which had already been ball-milled for 4.5 h, and subsequently ball-milled for an additional half hour. All materials handling was performed in an argon-filled glove box. The powder ball-milling was performed in a stainless steel vial with 55 cm^3 internal volume sealed with Teflon O-rings. Five wolfram carbide (WC) balls with a diameter of approximately 10 mm and a total weight of about 31 g were used for the preparation of the samples. Three grams of each sample was produced with the weight ratio of ball to powder as 10:1. The samples were characterized with X-ray powder diffraction (XRPD) using a Bragg−Brantano STOE diffractometer (40 kV, 30 mA, CuK_α with $\lambda = 1.5418$ Å). The sample powders were placed in a specially designed airtight sample holder with an aluminum foil X-ray window and a Si reference under inert gas protection in a glove box.

The X-ray powder diffraction spectra of doped/undoped Na_3AlH_6 (see Figure 1) show a very high rate of conversion because the $NaAlH_4$ peaks are absent and only small peaks of NaH (decomposed Na_3AlH_6) are seen.

In the present work, the quasielastic neutron scattering (QENS) technique was employed to investigate the hydrogen dynamics in Na_3AlH_6. QENS experiments were performed on the high-resolution backscattering spectrometer (BSS) located at the Forschungszentrum Jülich. The backscattering geometry for both monochromator and analyzer was employed to obtain an energy resolution of 0.8 μeV fwhm, making it possible to resolve quasielastic broadening of approximately 0.1 μeV.

Doppler-shifting the incident neutrons by rapidly moving the monochromator crystals changed the incident energy, E_i. The setup had energy transfers of ± 17 μeV. With the Si(111) monochromator and analyzer, a neutron wavelength of $\lambda = 6.271$ Å was selected. Ten helium counters, which were located very close to the sample, recorded the analyzed neutrons simultaneously.

The samples were loaded in flat $0.1 \times 30.0 \times 40.0$ mm^3 Al containers sealed with indium wire. The sample thickness was chosen to minimize multiple-scattering effects. The powder-filled containers were oriented close to 45° with respect to the incident beam. The spectra were recorded by ten detectors that correspond to a range of scattering vectors of $q = 0.16-1.87$ Å^{-1}. The instrumental resolution functions were determined from the measured QENS spectra of each sample at low temperature ($T = 30$ K).

Because of the large incoherent scattering cross-section for hydrogen,[27] QENS is an optimal technique to study hydrogen dynamics because almost all signal stems from hydrogen atoms. The measured neutron scattering intensity in the experiment is proportional to the dynamical structure factor $S(q,\omega)$, which is a sum of coherent and incoherent contributions:

$$S(q,\omega) = S_{coh}(q,\omega) + S_{inc}(q,\omega) \tag{4}$$

in which q is the scattering vector and $\hbar\omega$ is the energy transfer. $S(q,\omega)$ is understood as the powder average of $S(\boldsymbol{q},\omega)$:

$$S(q,\omega) = \frac{1}{4\pi}\int \mathrm{d}\Omega S(\boldsymbol{q},\omega) \tag{5}$$

The incoherent scattering function $S_{inc}(\boldsymbol{q},\omega)$ is the space and time Fourier transform of the self-correlation function $G_s(\boldsymbol{r},t)$, describing the probability that a particle, which at time $t_0 = 0$ is located at the origin, is found at position $\boldsymbol{r}$ at time t. $S_{inc}(\boldsymbol{q},\omega)$ also can be expressed in terms of the intermediate scattering function $I(\boldsymbol{q},t)$:

$$S(\boldsymbol{q},\omega) = \int \mathrm{d}t\, I(\boldsymbol{q},t)\exp(i\omega t) \tag{6}$$

$$I(\boldsymbol{q},t) = \int \mathrm{d}^3 r\, G_s(\boldsymbol{r},t)\exp(i\boldsymbol{q}\boldsymbol{r}) \tag{7}$$

with $I(\boldsymbol{q},t)$ being the space Fourier transform of the self-correlation function $G_s(\boldsymbol{r},t)$. For small q, this space Fourier transform has the form of $I(\boldsymbol{q},t) = \exp(-q^2 D t)$, which represents an exponential decay in time (D is the diffusion constant). The time Fourier transform then has a Lorentzian line shape:

$$S_{inc}(q,\omega) = \frac{1}{\pi}\frac{Dq^2}{(Dq^2)^2 + \omega^2.} \tag{8}$$

This expression has a peak at $\omega = 0$ with a width (hwhm) of

$$\Gamma = Dq^2. \tag{9}$$

For large q, eq 9 generally is not valid because the diffusion cannot be considered continuous. The finite steps of diffusing atoms in lattices are taken into account by the Chudley−Elliott model.[28] For long-range diffusion of hydrogen atoms, Γ is given for large q by

$$\Gamma(q) = \frac{6D}{L^2}\left(1 - \frac{\sin qL}{qL}\right) \tag{10}$$

for a fixed hydrogen jump length L and a hydrogen diffusion constant for a spherical jump distribution

$$D = \frac{L^2}{6\tau}. \tag{11}$$

When a quasielastic component is present, the spectra are fitted to the model of an incoherent scattering function:

$$S^{tot}_{inc}(q,\omega) = R(q,\omega) \otimes (B_0\delta(\omega) + B_1 L_0(\omega,\Gamma)) + C_{backgr} \tag{12}$$

in which $\delta(\omega)$ is the elastic delta function, $L_0(\omega,\Gamma)$ is the quasielastic Lorentzian with an energy width (hwhm) Γ at $\omega = 0$, B_0 is the elastic incoherent signal, and C_{backgr} is the constant background term. The ratio of the amplitudes $B_1/(B_0+B_1)$ determines the fraction of mobile hydrogen atoms. The convolving function $R(q,\omega)$ is the instrumental resolution function, which for this instrument is modeled well by the sum of one Gaussian and two Lorentzians with half widths σ_1, σ_2, and σ_3, respectively:

$$R(q,\omega) = A_1 G_1(\omega,\sigma_1) + A_2 L_1(\omega,\sigma_2) + A_3 L_2(\omega,\sigma_2). \tag{13}$$

4. Results and Discussion

Hydrogen diffusion through the bulk toward the surface is important for fast desorption from the material. This type of process is either mediated by hydrogen interstitials or vacancies.

4.1 DFT Results. From the DFT calculations, we find the formation energy of hydrogen interstitials to be very high: 2.42 eV for undoped Na_3AlH_6. For Ti@Al-doped Na_3AlH_6, the energy is also high, but it depends on the distance to titanium. Away from Ti, molecular hydrogen forms (due to weakened Al−H bonds caused by Ti), whereas the formation energy of an interstitial next to titanium is 0.74 eV plus the high cost of the Ti substitution (see below).

Hydrogen diffusion in Na_3AlH_6 is therefore expected to be mediated by hydrogen vacancies, which diffuse between neighboring $(AlH_5)^{2-}$ and $(AlH_6)^{3-}$ groups (see Figure 2a).

Deposition of titanium atoms into the alanate matrix is done by bulk substitution of Ti@Al-sites. In the bulk, the Al-sites are found to be preferred over Na sites, in agreement with existing calculations[19] also using the cohesive energies of aluminum, sodium, and titanium as references. For Ti@Al sites, the calculated substitution energy is 0.95 eV, for Ti@2*b*-Na sites 2.44 eV, and for Ti@4*e*-Na sites 2.00 eV. Assuming Ti does bulk substitute for Al, an effect of titanium could be a lowering of the hydrogen vacancy formation energies. The DFT calculations result in a vacancy formation energy of 1.54 eV for undoped Na_3AlH_6. Depending on the site, the formation energy for a hydrogen vacancy in the $(AlH_6)^{3-}$ groups surrounding titanium in $Na_{24}(Ti@Al)Al_7H_{48}$ can be as low as 1.38 eV.

Taking into account the energy required for the Ti@Al substitution (0.95 eV), the hydrogen vacancy formation in pure Na_3AlH_6 is energetically cheaper. However, titanium substituting aluminum can act as a hydrogen-trapping site, thereby creating a hydrogen vacancy by transferring a distant hydrogen atom close to titanium, which is comparatively cheap: 0.26 eV (distance Ti−H initially 7.2 Å). With an energy of 0.95 eV for the substitution of aluminum by titanium, the total cost for this local hydrogen vacancy formation without removing a hydrogen atom from the bulk is 1.21 eV, i.e., 0.33 eV less expensive compared to hydrogen vacancy formation in undoped Na_3AlH_6.

Figure 2b shows the diffusion of a hydrogen atom from an $(AlH_6)^{3-}$ to an $(AlH_5)^{2-}$ group in titanium-doped Na_3AlH_6 (titanium substituting aluminum: $Na_{24}(Ti@Al)Al_7H_{48}$). The activation energies obtained from the NEB calculations are quite

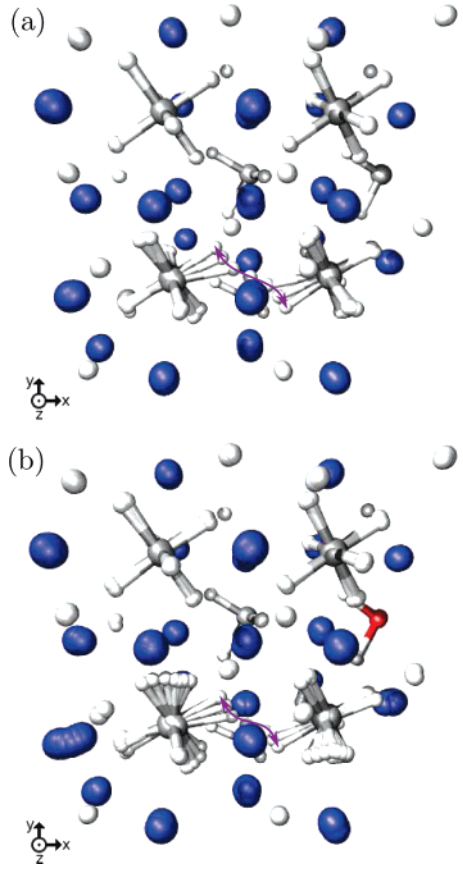

Figure 2. Long-range hydrogen diffusion path in (a) $Na_{24}Al_8H_{47}$ and (b) $Na_{24}(Ti@Al)Al_7H_{47}$. Representing colors: sodium, blue; aluminum, gray; titanium, red; hydrogen, white.

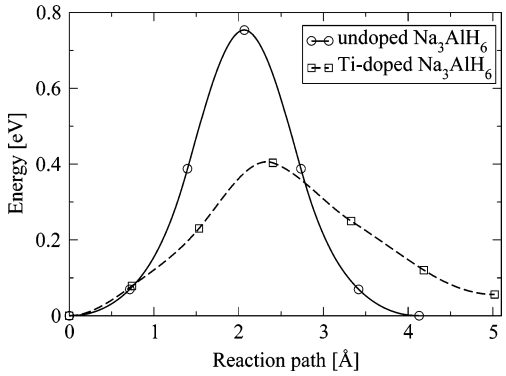

Figure 3. Minimum energy paths for long-range hydrogen diffusion in undoped and titanium-doped Na_3AlH_6.

high for undoped Na_3AlH_6: $E_a = 0.75$ eV or higher. There are two possible hydrogen diffusion paths with jump lengths around 3.0 Å having barriers of the order of 0.8−0.9 eV and three paths at 3.1−3.2 Å with higher barriers around 1.0 eV. For Ti@Al-doped Na_3AlH_6, the barrier can be significantly lower, depending on the diffusion path and the distance to the titanium dopant. Barriers as low as 0.36 eV are found (see Figure 3), although these are only accessible to a small fraction of the hydrogen atoms (<1% for ∼4 mol % $TiCl_3$ dopant). The corresponding hydrogen jump lengths are 3.08 and 2.80 Å for the undoped and titanium-doped system, respectively. Jumps directly to and from titanium are not considered because titanium binds additional hydrogen atoms quite strongly and hence does not promote hydrogen diffusion.

We continue by comparing these findings to the experimental observations from the QENS experiments.

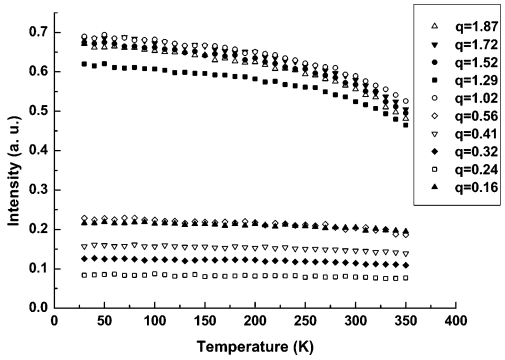

Figure 4. Elastic temperature scans on undoped Na_3AlH_6.

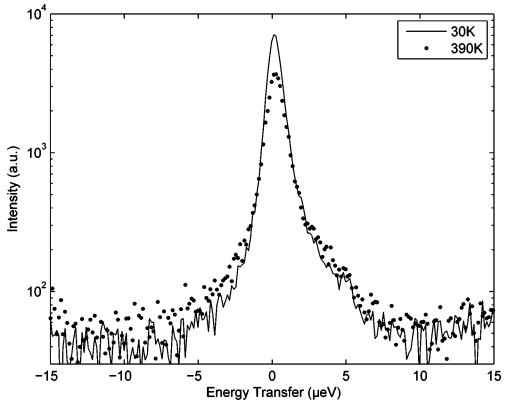

Figure 5. QENS spectra with $q = 1.87$ Å^{-1} for undoped Na_3AlH_6 measured at $T = 30$ and 390 K, respectively.

4.2. QENS Data. Elastic temperature scans at $\hbar\omega = 0$ on doped and undoped Na_3AlH_6 at 30−350 K (see Figure 4) show a roughly linear decrease in intensity with T up to ∼250 K and a Debye−Waller q dependence.[29] Above this value, there is a downward curvature, indicating that intensity is transferred to the inelastic regions. QENS spectra of undoped Na_3AlH_6 were measured at 150, 250, 350, and 390 K, and the doped samples at 300 and 350 K. QENS spectra with $q = 1.87$ Å^{-1} for undoped Na_3AlH_6 measured at $T = 30$ and 390 K are shown in Figure 5.

The spectra in Figure 5 show limited quasielastic broadening for undoped Na_3AlH_6 at 390 K, best seen in the tails at ±2−4 μeV. At lower temperatures, effectively no broadening was observed in the undoped samples.

The hydrogen atoms are assumed to be frozen at low temperature ($T = 30$ K), thus the instrumental resolution function for each value of q was determined by fitting the QENS spectrum with a quasielastic Lorentzian amplitude of zero in eq 12. The QENS spectra at higher temperatures were fitted with fixed resolution parameters and free values of Γ, B_0, B_1, and C. The q dependence of the quasielastic Lorentzian halfwidths as a function of scattering vectors is shown for undoped Na_3AlH_6 at 390 K (Figure 6) and doped Na_3AlH_6 at 350 K (Figure 7). Because of a lower signal intensity and thus higher uncertainty at low q values in the present work, the ratio of the amplitudes $B_1/(B_0+B_1)$, i.e., the fraction of mobile hydrogen atoms, determined at high q was used as a fixed value when data fitting at low q.

4.3. Combined Data Analysis. An accurate fit of the QENS data for undoped Na_3AlH_6 at $T = 390$ K to the Chudley−Elliott diffusion model (see Figure 6) yields a hydrogen jump length of $L \simeq 2.80$ Å and an inverse jump rate $\tau = 2.35$ ns. At this temperature, 13% of the hydrogen was found to be mobile. Because the diffusion is vacancy mediated, it must be taken

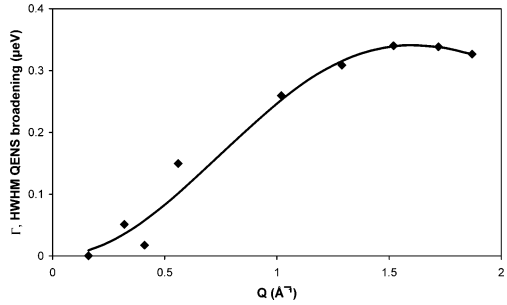

Figure 6. Quasielastic broading vs scattering angle for undoped Na_3AlH_6 at $T = 390$ K (solid line: fit to Chudley−Elliott diffusion model).

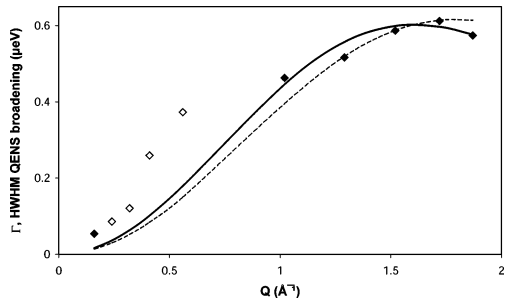

Figure 7. Quasielastic broadening vs scattering angle for titanium-doped Na_3AlH_6 at $T = 350$ K (solid line: Chudley−Elliott fit for long-range diffusion; dashed line: Chudley−Elliott fit for localized hydrogen dynamics in the undoped system; empty diamonds: low-intensity resulting in high uncertainty in Γ).

into account that only the motion of the vacancy can be considered as a random walk, while the involved atomic motions are correlated (see, e.g., ref 30). In a zero-order approximation, i.e., one atomic jump per vacancy diffusion step, the only effect is a rescaling of τ.[31] The uncertainty on τ might therefore be significant, but even a 50% error in τ only results in an error of $k_BT/2$ in the activation energy, corresponding to ~20 meV at 390 K.

Using a hTST prefactor of $\tau_0^{-1} = 2.23 \times 10^{13}$ s^{-1} obtained from a vibrational analysis of the initial and transition state of an internal hydrogen diffusion path using DFT calculations, we obtain an activation energy of 0.37 eV from the Chudley−Elliott fit. This barrier is much lower than the activation energies calculated using DFT for diffusional processes in undoped Na_3AlH_6. Because the QENS data for undoped Na_3AlH_6 did not show signatures of hydrogen motion corresponding to jump lengths and activation energies obtained from the DFT calculations for long-range diffusion (cf. Table 2), we continued to investigate localized events, i.e., vacancy-mediated hydrogen jumps on the same $(AlH_5)^{2-}$ complex. This is supported by a q dependent elastic incoherent structure factor[32] as opposed to $NaAlH_4$,[33] indicating spatial localization of the diffusing species in undoped Na_3AlH_6. These localized events will not contribute to macroscopic hydrogen diffusion.

The QENS data was found to be in good agreement with our DFT results for hydrogen jumps in the same $(AlH_5)^{2-}$ group (see Figure 8), where the calculated activation energy is 0.41 eV and the corresponding jump length $L = 2.50$ Å. The calculated barrier for long-range diffusion is at least 0.75 eV.

For titanium-doped Na_3AlH_6, a Chudley−Elliott fit for $T = 350$ K (see Figure 7) using a calculated prefactor of $\tau_0^{-1} = 2.13 \times 10^{13}$ s^{-1} results in an activation energy of 0.31 eV. In this case, the fraction of mobile hydrogen is found to be as low as 2%. This value was fixed based on an average of the high q results, but the broadening is sensitive to this fraction. The lower barrier could stem from long-range hydrogen diffusion near a

TABLE 2: Experimental and Theoretical Results for Hydrogen Diffusion in Undoped and Ti-Doped Na_3AlH_6[a]

	$\tau^{-1}(T)$ [GHz]	L [Å]	E_a [eV]	mobile fraction [%]
undoped samples − $T = 390$ K				
QENS	0.4	2.80	0.37	13
DFT_D	9×10^{-6}	3.08	0.75	
DFT_L	0.1	2.50	0.41	
doped samples − $T = 350$ K				
QENS	0.8	2.80	0.31	2
DFT_D	0.1	2.80	0.36	
DFT_L	no well-defined local H dynamics path (H trapped by Ti)			

[a] The theoretical results for localized events and long-range diffusion are labeled DFT_L and DFT_D, respectively. The QENS values for the activation energies have been calculated using DFT results for the prefactors τ_0^{-1}

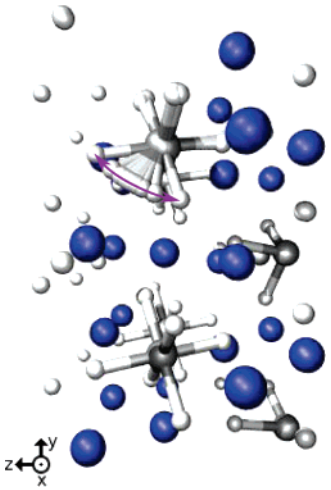

Figure 8. Local hydrogen dynamics path in $Na_{24}Al_8H_{47}$.

Ti@Al dopant with a calculated activation energy of $E_a = 0.36$ eV and a jump length of $L = 2.80$ Å. The broadening is more likely explained by localized dynamics in undoped Na_3AlH_6 with a jump length of 2.50 Å (see Figure 7) because only a slightly higher fraction of mobile hydrogen is observed for Ti-doped Na_3AlH_6. In undoped Na_3AlH_6 at 350 K, less than 1% of the hydrogen appears to be mobile, but it was not possible to determine the broadening as a function of q due to the weak intensity. The observed broadening appears to be similar for undoped and doped Na_3AlH_6 samples at 350 K.

It should be noted that for localized, low barrier jumps between interstitial sites in other systems with higher symmetry, e.g., as observed in Laves phase materials,[34] one would expect a q independent broadening at large q for localized events.[35,36] However, according to the model of successive oscillatory and diffusive motion by Singwi and Sjölander,[37] a smaller diffusion rate can lead to a q dependent broadening also for larger q.[33] Our DFT calculations result in a prefactor for local H dynamics in Na_3AlH_6 of $\tau_0^{-1} = 2.23 \times 10^{13}$ s^{-1}, which is 2 orders of magnitude smaller than prefactors for localized events in the Laves phase materials.[34] With an activation energy of 0.37 eV for hydrogen dynamics in Na_3AlH_6 being at least twice as large compared to activation energies for localized dynamics in the Laves phase materials,[34] the jump rate at, e.g., 390 K, is at least 5 orders of magnitude smaller for localized events in Na_3AlH_6. The broadening is therefore still q dependent for larger q compared to the Laves phase materials.

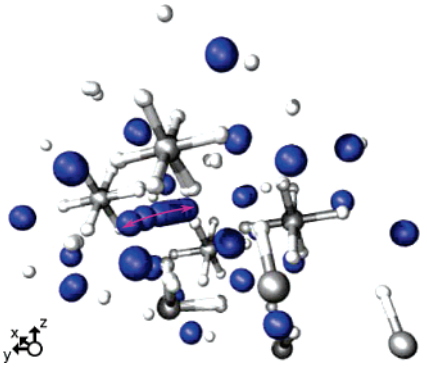

Figure 9. Sodium diffusion path between a 4*e* and a 2*b* sodium vacancy site.

Only by combining the experimental QENS results, which show a Chudley−Elliott type broadening appearing to originate from a long-range diffusional process, with the dynamical parameters obtained from the DFT calculations, was it possible to correctly identify the observed hydrogen dynamics as localized events.

Because the QENS experiments clearly show no hydrogen dynamics with activation energies less than ∼0.3 eV, we continued to investigate (using only DFT calculations) alternative explanations to the observed point defect diffusion with an activation energy of 0.126 eV reported by Palumbo et al.[9]

For vacancy-mediated sodium diffusion from a 4*e* to a 2*b* site (see Figure 9), our DFT calculations yield an (asymmetric) activation barrier of 0.12 eV and a jump length of 2.51 Å. Vibrational analysis of the initial and transition state of this diffusion process yields a jump rate of 4.26×10^3 s^{-1} at the resonance temperature of $T = 70$ K, as observed by Palumbo et al.[9] For deuterated systems, a shift of the resonance temperature to $T = 77$ K was observed.[10] We have therefore studied the influence of deuteration on the pre-exponential factor of sodium diffusion. The higher mass of deuterium compared to hydrogen leads to lower vibrational frequencies of the deuterium atoms. In addition, the lattice constants of hydrides and deuterates can differ,[38,39] giving raise to more complicated influence on diffusion rates. The pre-exponential factor of the jump rate is mainly determined by the frequencies of the diffusing sodium atom. Therefore, corrections to the jump rate due to deuteration cannot simply be taken into account by considering the mass of deuterium for obtaining the frequencies from the Hessian matrix. In this case, anharmonic effects leading to different bond lengths compared to undeuterated systems are more important. We therefore estimate the effect of deuteration by calculating the minimum energy path of the vacancy-mediated sodium diffusion with the constraint of the Al−D bondlengths being held at their values determined by X-ray diffraction[20] (1.746, 1.758, and 1.770 Å).

Keeping the Al−D bondlengths fixed at nonequilibrium distances, we only consider the frequencies of the diffusing sodium atom at the initial and transition state. Only considering these frequencies, the prefactor of the jump rate for the deuterated system is 13% lower compared to the system without constraints on bond lengths (i.e., the undeuterated system). The resonance temperature shift can then be estimated using the exponential dependence of the jump rate on the temperature (eq 2) and that jump rate and angular vibration frequency are equal at anelastic resonance.[10] Assuming the activation energy to be 0.01 eV higher for the deuterated system than for the undeuterated system (as measured by Palumbo et al.[10]), we obtain a shift of the resonance temperature to $T = 76$ K.

Besides the lowered formation energies for local hydrogen vacancies in Ti-doped Na_3AlH_6, the formation of hydrogen vacancies is favorable close to sodium vacancies (see also ref 19). The formation energy for a sodium vacancy at 2*b*-Na sites in undoped Na_3AlH_6 is 2.65 eV (and 0.24 eV higher for 4*e*-Na sites). The formation of a hydrogen vacancy close to the sodium vacancy means a gain of 1.32 eV. Hence, the overall energy for such a hydrogen vacancy is only 1.34 eV. This might be an initial reaction path of the decomposition of Na_3AlH_6.

4.4. Discussion. Palumbo et al.[9] have reported point defect motion with a low activation energy of 0.126 eV, detected by anelastic spectroscopy with 5×10^3 jumps/s at a resonance temperature of $T = 70$ K for both undoped and titanium-doped sodium alanate. They observe these mobile defects in thermally treated and compacted disc samples and conclude that they are most likely due to hydrogen vacancy dynamics in the Na_3AlH_6 phase.[10]

The lowest activation energies for hydrogen diffusion we have determined by DFT are much larger: 0.41 eV for local hydrogen dynamics in Na_3AlH_6 and 0.36 eV for long-range diffusion in Ti-doped Na_3AlH_6. Furthermore, the QENS data, being "selective" to hydrogen motion, shows no signatures of diffusion below $T = 250$ K (i.e., with activation barriers less than ∼0.3 eV) in either undoped or titanium-doped Na_3AlH_6.

On the basis of DFT calculations and QENS data, we conclude that the observed point defect motion at 70 K is probably not related to bulk hydrogen diffusion. Below ≤250 K, the elastic signal (see Figure 4) lacks features which would result from a diffusion broadening larger than 0.1 μeV. With a proposed rate of 5×10^3 s^{-1} at $T = 70$ K and the 0.8 μeV resolution of the backscattering spectrometer, diffusing point defects involving hydrogen should yield 1−2 μeV broadening in doped and undoped samples alike[10] at 150 K. However, at this temperature, no broadening was observed in the QENS data. Considering other possible mobile species, our DFT results for sodium vacancy diffusion could account for the anelastic resonance at 70 K, yielding a jump rate of 4.26×10^3 s^{-1} at this temperature and an activation barrier of 0.12 eV. This agreement with the experimental results of Palumbo et al.[9] is further supported by consistence with respect to a shift of the resonance temperature to 77 K for deuterated sodium alanate.[10]

Because no hydrogen diffusion with barriers below 0.3 eV is observed using QENS or DFT in either $NaAlH_4$[33] or Na_3AlH_6, doped or undoped, we propose that the observed point defect motion could be related to diffusion of sodium or other non-hydrogen species in Na_3AlH_6. Second, the feature could be inherent from the thermal treatment procedure or stem from the compacted nature of the samples. More work is needed to clarify this.

5. Conclusion

With a combined experimental and theoretical approach, we are able to fully analyze hydrogen dynamics in sodium alanate. For undoped Na_3AlH_6, long-range hydrogen diffusion is energetically expensive (activation energies of ∼0.8 eV). The QENS results for undoped Na_3AlH_6 with an activation barrier of ∼0.4 eV can therefore only be attributed to localized hydrogen vacancy dynamics within the same $(AlH_5)^{2-}$ group where the calculated barriers agree well. This clearly illustrates the synergy of the integrated theoretical and experimental approach because an independent QENS analysis of the Chudley−Elliott type behavior would have led to the conclusion of long-range hydrogen diffusion.

If titanium does bulk substitute, the activation barriers for long-range hydrogen diffusion could be significantly lower (on

the order of 0.4 eV). In this case, the QENS data fit the DFT results for such a long-range process quite well. However, the experimental results can be explained by localized hydrogen dynamics as well. Given the high cost of bulk substitution of Ti atoms combined with an only slightly higher fraction of mobile hydrogen for Ti-doped Na_3AlH_6 observed at 350 K and the lack of experimental confirmations of lattice expansions due to Ti,[11] it is unlikely that bulk-substituting titanium[8] can explain the improved desorption kinetics as a result of improved bulk diffusion of hydrogen.

In our QENS experiments, we have only observed hydrogen dynamics with activation energies of about 0.3−0.4 eV. We propose that the low-temperature point defect diffusion reported by Palumbo et al.[9] at 0.126 eV either involves sodium diffusion in Na_3AlH_6 or it is inherent from the thermal treatment or sample compaction processes.

Acknowledgment. We thank Prof. Jens Kehlet Nørskov, Dr. Christian Bahl, Dr. Luise Theil Kuhn, Dr. Dennis Engberg, and Dr. Anders Andreasen for valuable discussions. We acknowledge financial support by the NABIIT program and the DANSCATT instrument center funded by the Danish Research Councils. This research project has been supported by the European Commission under the sixth Framework through the Key Action: Strengthening the European Research Area, Research Infrastructures, Contract no. RII3-CT-2003-505925. We acknowledge the Danish Center for Scientific Computing (DCSC) for supercomputer access.

References and Notes

(1) Bogdanović, B.; Schwickardi, M. *J. Alloys Compd.* **1997**, *253*−*254*, 1.
(2) Ke, X.; Tanaka; I. *Phys. Rev. B* **2005**, *71*, 024117.
(3) Bellosta von Colbe, J. M.; Schmidt, W.; Felderhoff, M.; Bogdanović, B.; Schüth, F. *Angew. Chem., Int. Ed.* **2006**, *45*, 3663.
(4) Brinks, H. W.; Sulic, M.; Jensen, C. M.; Hauback, B. C. *J. Phys. Chem. B* **2006**, *110*, 2740.
(5) Kuba, M. T.; Eaton, S. S.; Morales A.; Jensen, C. M. *J. Mater. Res.* **2005**, *20*, 3265.
(6) Vegge, T. *Phys. Chem. Chem. Phys.* **2006**, *8*, 4853.
(7) Schüth, F.; Bogdanović, B.; Felderhoff, M. *Chem. Commun.* **2004**, *2249*.
(8) Sun, D.; Kiyobayashi, T.; Takeshita, H. T.; Kuriyama, N.; Jensen, C. M. *J. Alloys Compd.* **2002**, *337*, L8.
(9) Palumbo, O.; Cantelli, R.; Paolone, A.; Jensen, C. M.; Srinivasan, S. S. *J. Alloys Compd.* **2005**, *404*−*406*, 748.
(10) Palumbo, O.; Paolone, A.; Cantelli, R.; Jensen, C. M.; Sulic, M. *J. Phys. Chem. B* **2006**, *110*, 9105.
(11) Brinks, H. W.; Jensen, C. M.; Srinivasan, S. S.; Hauback, B. C.; Blanchard, D.; Murphy, K. *J. Alloys Compd.* **2004**, *376*, 215.
(12) Kohn, W.; Sham, L. J. *Phys. Rev.* **1965**, *140*, A1133.
(13) Hammer, B.; Hansen, L. B.; Nørskov, J. K. *Phys. Rev. B* **1999**, *59*, 7413.
(14) Vanderbilt, D. *Phys. Rev. B* **1990**, *41*, R7892.
(15) Perdew, J. P.; Chevary, J. A.; Vosko, S. H.; Jackson, K. A.; Pederson, M. R.; Singh, D. J.; Fiolhais, C. *Phys. Rev. B* **1992**, *46*, 6671.
(16) Atomic Simulation Environment, https://wiki.fysik.dtu.dk/ase.
(17) Peles, A.; Alford, J. A.; Ma, Z.; Yang, L.; Chou, M. Y. *Phys. Rev. B* **2004**, *70*, 165105.
(18) Vajeeston, P.; Ravindran, P.; Kjekshus, A.; Fjellvåg, H. *Phys. Rev. B* **2005**, *71*, 092103.
(19) Li, S.; Jena, P.; Ahuja, R. *Phys. Rev. B* **2006**, *73*, 241107.
(20) Rönnebro, E.; Noréus, D.; Kadir, K.; Reiser, A.; Bogdanović, B. *J. Alloys Compd.* **2000**, *299*, 101.
(21) Jónsson, H.; Mills, G.; Jacobsen, K. W. In *Classical and Quantum Dynamics in Condensed Phase Simulations*; Berne, B. J., Ciccoti, G., Coker, D. F., Eds.; World Scientific: Singapore, 1998.
(22) Maragakis, P.; Kaxiras, E.; Andreev, S.; Brumer, Y.; Reichman, D. R. *J. Chem. Phys.* **2002**, *117*, 4651.
(23) Hänggi, P.; Talkner, P.; Borkovec, M. *Rev. Mod. Phys.* **1990**, *62*, 251.
(24) Vegge, T. *Phys. Rev. B* **2004**, *70*, 034512.
(25) Vegge, T.; Rasmussen, T.; Leffers, T.; Pedersen, O. B.; Jacobsen, K. W. *Phys. Rev. Lett.* **2000**, *85*, 3866.
(26) Huot, J.; Boily, S.; Güther, V.; Schulz, R. *J. Alloys Compd.* **1999**, *283*, 304.
(27) Dianoux, A.-J.; Lander, G. *Neutron Data Booklet*; Old City: Philadelphia, 2003.
(28) Chudley, C. T.; Elliott, R. J. *Proc. Phys. Soc.* **1961**, *77*, 353.
(29) Squires, G. L. *Thermal Neutron Scattering*; Cambridge University Press: New York, 1978.
(30) Manning, J. R. *Diffusion Kinetics for Atoms in Crystals*; Van Nostrand: Princeton, NJ, 1968.
(31) Bender, O.; Schroeder, K. *Phys. Rev. B* **1979**, *19*, 3399.
(32) Bée, M. *Physica B* **1992**, *182*, 323.
(33) Shi, Q.; Voss, J.; Jacobsen, H. S.; Zamponi, M.; Lefmann, K.; Vegge, T. to be published.
(34) Skripov, A. V.; Voyevodina, L. S.; Hempelmann, R. *Phys. Rev. B* **2006**, *73*, 014302.
(35) Hall, P. L.; Ross, D. K. *Mol. Phys.* **1981**, *42*, 673.
(36) Bée, M. *Quasielastic Neutron Scattering*; Hilger: Bristol, U.K., 1988.
(37) Singwi, K. S.; Sjölander, A. *Phys. Rev.* **1960**, *119*, 863.
(38) Frankcombe, T. J.; Kroes, G.-J. *Phys. Rev. B* **2006**, *73*, 174302.
(39) Schirber, J. E.; Morosin, B. *Phys. Rev. B* **1975**, *12*, 117.